Journal of Fluids and Structures (1998) **12,** 561–590
Article No: fl980155

AN EFFECT OF TURBULENCE ON FLUIDELASTIC INSTABILITY IN TUBE BUNDLES: A NONLINEAR ANALYSIS

G. RZENTKOWSKI†
Ontario Hydro Technologies, Toronto, Ont., Canada

AND

J. H. LEVER
Cold Regions Research and Engineering Laboratory Hanover, New Hampshire, U.S.A.

(Accepted 6 March 1996 and in revised form 13 January 1998)

This paper is concerned with the behaviour of a tube bundle subjected to combined fluidelastic and turbulence excitation. Here, we formulate the fluidelastic forces based on a simplified, nonlinear model for a single flexible tube surrounded by rigid neighbours and constrained to move transverse to the mean flow. We use a flat power spectral density function to express the turbulence excitation. The resulting system we first examine heuristically, based on a superposition of both excitation mechanisms. We then assess the merits of this approach via direct numerical integration of the equation of motion. Lastly, we perform a nonlinear investigation into the sensitivity of the fluidelastic stability boundary on variations in the random field of turbulence and generate a stability map. The analysis shows that the fluidelastic stability boundary defined by an unstable bifurcation may be reduced by turbulence; for long-term operation, the threshold reduction may approach the size of a hysteresis region. This effect increases with turbulence intensity and decreases with unstable-limit-cycle amplitude. For a stable bifurcation, the fluidelastic stability boundary is virtually unaffected by turbulence. In the latter case, the effect of turbulence is through practical stability definitions made using amplitude–response curves.

1. INTRODUCTION

CROSS-FLOW-INDUCED VIBRATIONS OF TUBE BUNDLES affect the operation of a variety of industrial equipment, particularly associated with power generation technology (e.g. heat exchangers and steam generators). Mechanical failures have occurred after several years of service, due to small-amplitude oscillations caused by turbulence, or after short periods of time due to large-amplitude, self-excited oscillations. Both excitation mechanisms have been the subject of extensive experimental and analytical research, leading to predictive models and design guidelines [see, for example, Pettigrew (1981), Païdoussis (1983), Chen (1984), Singh & Soler (1984) and Weaver & Fitzpatrick (1987)]. Researchers have also attempted to identify the interaction effect between turbulence and fluidelastic instability. This, however, has not yielded consistent results, particularly in the practical estimation of the fluidelastic stability boundary.

† Present address: Atomic Energy Control Board, 280 Slater Street, Ottawa, Ont., Canada.

0889-9746/98/050561 + 30 $30.00

Early experimental studies by Southworth & Zdravkovich (1975), Franklin & Soper (1977), and Chen & Jendrzejczyk (1981) indicated that turbulence may either increase or decrease the critical flow velocity for fluidelastic instability, depending on the turbulence characteristics. In all cases, researchers positioned turbulence generators upstream of the tested bundles. More recently, Price *et al.* (1986, 1987) performed a detailed experimental investigation and found that the presence of turbulence generators has little or no effect on the onset of fluidelastic instability. The authors concluded that the interstitial flow characteristics beyond the first few rows are governed by the bundle itself, independent of upstream conditions. This finding makes it difficult to investigate experimentally the interaction between turbulence and fluidelastic instability in tube bundles. Here, we explore a theoretical approach.

In our previous theoretical work (Lever & Rzentkowski 1989), we examined the influence of turbulence on fluidelastic instability in tube bundles through interpretation of amplitude–response curves. Since this was a linearized analysis, the two excitation mechanisms were superimposed and any coupling effect was omitted. Nevertheless, we showed that increasing turbulence reduced the apparent stability boundary for fluidelastic instability, utilizing amplitude–response curves; the size of the reduction depended on the practical threshold definition used. This observation, to a certain extent, may explain the contradictory results from the aforementioned experimental studies of the problem.

In the present study, we extend this analysis by formulating a nonlinear model for combined fluidelastic and turbulence excitation of tube bundles. We represent the tube as a simple, third-order, fluidelastic oscillator and investigate the effect of turbulence on the location of bifurcation points. To establish the model, the study is focused on the simplest physical system while retaining the behaviour of full bundles. We thus utilize the nonlinear, one-dimensional flow equations, from the linearized, steady-state "tube-in-channel-flow" model of Lever & Weaver (1982) for a single flexible tube surrounded by rigid neighbours, to express the fluidelastic force. We chose this model because it is relatively simple and yields good agreement with experimental data for parallel triangular and square arrays, where flow curvature is small and the assumption of one-dimensional flow is reasonable. We realize that some of the assumptions of the model may not be valid for large tube motion. It must be appreciated, however, that a more rigorous treatment of the underlying fluid dynamics requires formulation of a new theory which we feel is beyond the scope of the present study, which is to investigate the role of turbulence in triggering fluidelastic instability. This is especially true since, in the vicinity of the fluidelastic stability threshold, tube motion is of a small amplitude. Moreover, this reformulated nonlinear theory was already examined by the authors (Rzentkowski & Lever 1992) and, after some modifications to the flow redistribution mechanism which accounts for most of the modelled characteristics of fluidelastic instability, was found to give good agreement with test data. We thus feel that, because of its simple form and the correct assessment of a post-stable behaviour of a tube bundle (stable versus unstable limit cycle), the theory provides a convenient analytical platform to include and examine the effects of turbulence, and thus, to achieve the objective of this study. Here, we use a power spectral density function to formulate the turbulence force acting on the tube. Based on experimental evidence (Pettigrew & Gorman 1978), we assume that this function is constant (white noise) and proportional to the square of flow dynamic head over the frequency range of interest.

The resulting system we first examine heuristically via superposition of the two forcing mechanisms: a third-order fluidelastic solution (limit cycle) and a linear response curve due to combined excitation. Based on this idealized representation, we develop an analytical

expression which approximately defines the location of the fluidelastic stability boundary for coupled excitation. We also use a direct numerical integration of the equation of tube motion to obtain a fully nonlinear solution. We compare the two solutions and use them subsequently to study the sensitivity of the fluidelastic stability boundary governed by an unstable bifurcation to variations in the random field of turbulence. Since the analytical prediction agrees well with the numerical one, we apply it further to examine the effect of unstable-limit-cycle amplitude and of the time of equipment operation on the fluidelastic stability threshold. We also generate a theoretical stability map to compare the linear and nonlinear stability boundaries over a wide range of mass-damping parameters.

Using this theoretical approach, we show that the interaction mechanism between fluidelastic instability and turbulence is dependent on the tube nonlinear characteristics. For an unstable bifurcation, the fluidelastic stability boundary may be reduced by turbulence; the threshold reduction may approach the size of a hysteresis region for long-term equipment operation. We observe that this effect increases with turbulence intensity and decreases with unstable-limit-cycle amplitude. For a stable bifurcation, the fluidelastic stability boundary is virtually unaffected; the effect of turbulence manifests itself through the interpretation of amplitude–response curves.

2. MODEL FORMULATION

We can examine theoretically the effect of turbulence on fluidelastic instability in tube bundles only to the extent that the underlying theoretical models represent the physics of each mechanism. In this study, we limit the modelling to a structurally linear tube which is surrounded by rigid neighbours and constrained to move transverse to the mean flow. Through the series of experiments on parallel triangular and square arrays (Lever & Rzentkowski 1993), we showed that, at least in the mass-damping parameter range tested ($\bar{m}\delta_0 = 1.9$ to 23.5), this simplified system displays similar post-stable behaviour to a fully flexible bundle. In addition, we assume here that the fluid forces, which consist of a nonlinear fluidelastic force, $F_E(t)$, a turbulence force, $F_T(t)$, and a linear fluid-damping force, $F_D(t)$, are fully correlated along the tube span. Thus, the simplified equation of motion may be written as

$$m_0\ddot{y}(t) + c_0\dot{y}(t) + k_0 y(t) = F_E(t) + F_T(t) + F_D(t), \tag{1}$$

where m_0, c_0 and k_0 are, respectively, the structural mass, damping, and stiffness coefficients, and $y(t)$ is transverse-to-flow tube displacement.

2.1. Fluidelastic Force

We express the nonlinear, fluidelastic forces based on the linearized, steady-state "tube-in-channel-flow" model initially developed by Lever & Weaver (1982). We chose this model because it is relatively simple and yields good agreement with experimental data for parallel triangular and square arrays, where flow curvature is small and the assumption of one-dimensional flow is reasonable. Because the original authors completely describe the underlying flow theory, we will discuss here only the fundamental assumptions of the model and the modifications necessary to formulate its nonlinear, time-domain extension. In our earlier study (Rzentkowski & Lever 1992), we already examined this reformulated nonlinear theory in an attempt to determine whether the original model of Lever & Weaver (1982)

would correctly predict observed post-stable behaviour of tube bundles. We found that, with some modifications, it gives good agreement with test data.

2.1.1. *Underlying flow theory*

Figure 1 shows the "unit cell" sufficient to describe the fluidelastic behaviour of a one-degree-of-freedom tube bundle. A single flexible tube is symmetrically located relative to the apparent position of neighbouring tubes and undergoes motion, $y(t)$, in the transverse-to-flow direction only. A highly regular flow field is assumed, with fluid flowing through the bundle without crossing from one flow channel to the next. The steady streamlines through the bundle define the boundaries of the "unit cell". The streamtubes are narrow relative to their length, so that one-dimensional flow assumption can be used.

For incompressible, one-dimensional flow, we may write the area, velocity and pressure variation along the two streamtubes as the sum of first-order functions of position only, plus second-order perturbation functions (containing linear and nonlinear terms) of both position and time. Employing symmetry, the resulting expressions become

$$\begin{aligned} A_i(s,t) &= \bar{A}(s) + (-1)^{i+1}a(s,t), \quad a(s,t) < \bar{A}(s), \\ U_i(s,t) &= \bar{U}(s) + (-1)^{i+1}u(s,t), \quad u(s,t) < \bar{U}(s), \\ P_i(s,t) &= \bar{P}(s) + (-1)^{i+1}p(s,t), \quad p(s,t) < \bar{P}(s), \end{aligned} \tag{2}$$

where the subscript $i = 1$ and 2 refers to the left and right streamtube, respectively. For small-amplitude motion, the perturbation functions are significantly smaller than the first-order terms. For large-amplitude motion, tube clashing with a boundary limits the area perturbation and, therefore, the velocity and pressure perturbations.

Whereas Lever & Weaver (1982) assumed simple harmonic tube motion, the present formulation requires that the time dependence of $y(t)$ and the perturbation functions remain

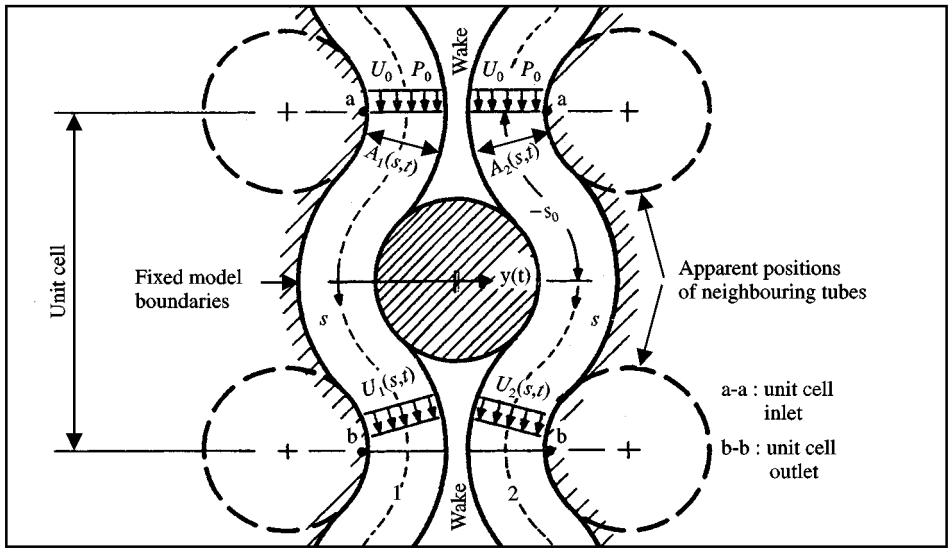

Figure 1. "Unit cell" for the fluidelastic model.

unspecified. As with the original model, we also assume that the streamtube area perturbation follows the tube motion but with a time lag, due to fluid inertia. Further, this time lag increases linearly with the distance along the streamtube from $\tau = 0$ at the tube centreline, $s = 0$, to $\tau = l/U_0$ at the "unit-cell" inlet, $s = -s_0$ (in the time lag formulation, l is the relevant fluid inertia length, and U_0 is the steady flow velocity at the inlet). Following these assumptions, we may write

$$a(s, t) = y\left(t + \tau\frac{s}{s_0}\right). \tag{3}$$

Note that, because the distance along the streamtube, s, is negative in the direction of the inlet, the area perturbation lags behind the tube motion, as required.

With the streamtube perturbation function specified, we may obtain the velocity and pressure variations using the one-dimensional, unsteady continuity and Bernoulli equations, respectively,

$$\int_{-s_0}^{s} \frac{\partial A}{\partial t}\,\partial s + A(s, t)U(s, t) = A(-s_0, t) \tag{4}$$

and

$$\frac{1}{\rho}\,\mathrm{P}(s, t) + \frac{1}{2}\,U^2(s, t) + \int_{-s_0}^{s} \frac{\partial U(s, t)}{\partial t}\,\mathrm{d}s + \frac{1}{2}\frac{h}{s_o}\int_{-s_0}^{s} U^2(s, t)\mathrm{d}s$$

$$= \frac{1}{2}\,U^2(-s_0, t) + \frac{1}{\rho}\,P(-s_0, t)\,, \tag{5}$$

where h is the flow resistance coefficient. As with the original model, we apply here the simplifying assumptions of constant area streamtubes, $\bar{A}(s) = A_0$, and no velocity and pressure fluctuation at the "unit cell" inlet, $u(-s_0, t) = p(-s_0, t) = 0$. Thus, after introducing the integration variable, $\xi = t + \tau s/s_0$, the solution of the continuity equation becomes

$$\frac{u(s, t)}{U_0} = \left(1 + \frac{s_0}{l}\right)\left[\frac{y(t_1) - y(t_2)}{A_o + y(t_2)}\right], \tag{6}$$

where $t_1 \equiv t - \tau$ and $t_2 \equiv t + \tau s/s_0$ are the time variables. To solve the Bernoulli equation, we expand this solution into a power series in $y(t_2)/A_0$. This series converges for $|y(t)| < A_0$ at $s = 0$, which is also the clashing limit with the "unit-cell" boundary. After series expansion, the unsteady velocity and pressure perturbation functions take the forms, respectively,

$$\frac{u(s, t)}{U_0} = (1 + s_0/l)\,[y(t_1) - y(t_2)] \sum_{n=0}^{\infty} [(-1)^n (1/A_0)^{n+1}\, y^n(t_2)]\,, \tag{7}$$

and

$$\frac{p(s, t)}{\rho U^2} = (1 + s_0/l)\Big\{(1 + s_0/l)\,[y(t_2) - y(t_1)] \sum_{n=0}^{\infty} [(-1)^n (1/A_0)^{n+1} y^n(t_2)]$$

$$+ 0{\cdot}5(1 + s_0/l)\,[y(t_1) - y(t_2)]^2 \sum_{n=1}^{\infty} [(-1)^n (1/A_0)^{n+1} n y^{n-1}(t_2)]$$

$$
\begin{aligned}
&- (1/U_0)\,\dot{y}(t_1) \sum_{n=0}^{\infty} \left[(-1)^n (1/A_0)^{n+1} \int_{-s_0}^{s} y^n(t_2)\,\mathrm{d}s \right] \\
&+ h/s_0 \left\{ \sum_{n=0}^{\infty} \left\{ (-1)^n (1/A_0)^{n+1} [0{\cdot}5(1 + s_0/l)\,n + 1] \int_{-s_0}^{s} y^{n+1}(t_2)\,\mathrm{d}s \right\} \right. \\
&- y(t_1) \sum_{n=0}^{\infty} \left\{ (-1)^n (1/A_0)^{n+1} [(1 + s_0/l)\,n + 1] \int_{-s_0}^{s} y^n(t_2)\,\mathrm{d}s \right\} \\
&\left. + 0{\cdot}5(1 + s_0/l)\,y^2(t_1) \sum_{n=1}^{\infty} \left[(-1)^n (1/A_0)^{n+1}\, n \int_{-s_0}^{s} y^{n-1}(t_2)\,\mathrm{d}s \right] \right\} \right\}, \qquad (8)
\end{aligned}
$$

where the subscript, n, yields the desired order of solution: $n = 0$ for linear and $n \geq 1$ for nonlinear.

Following the "tube-in-channel-flow" theory, we approximate the fluidelastic force acting on the tube as the pressure difference across its centreline, $p(0, t)$ times an equivalent area factor of flow attachment, D_E. As a result, the fluidelastic force per unit tube length becomes

$$
\begin{aligned}
F_E(t) = 2\rho D_E U_0^2 (1 + s_0/l) &\left\{ (1 + s_0/l)\,[y(t) - y(t_1)] \sum_{n=0}^{\infty} [(-1)^n (1/A_0)^{n+1}\, y^n(t)] \right. \\
&+ 0{\cdot}5(1 + s_0/l)\,[y(t_1) - y(t)]^2 \sum_{n=1}^{\infty} [(-1)^n (1/A_0)^{n+1}\, n y^{n-1}(t)] \\
&- (1/U_0)\,\dot{y}(t_1) \sum_{n=0}^{\infty} \left[(-1)^n (1/A_0)^{n-1} \int_{-s_0}^{0} y^n(t_2)\,\mathrm{d}s \right] \\
&+ h/s_0 \left\{ \sum_{n=0}^{\infty} \left\{ (-1)^n (1/A_0)^{n+1} [0{\cdot}5(1 + s_0/l)\,n + 1] \int_{-s_0}^{0} y^{n+1}(t_2)\,\mathrm{d}s \right\} \right. \\
&- y(t_1) \sum_{n=0}^{\infty} \left\{ (-1)^n (1/A_0)^{n+1} [(1 + s_0/l)\,n + 1] \int_{-s_0}^{0} y^n(t_2)\,\mathrm{d}s \right\} \\
&\left. \left. + 0{\cdot}5(1 + s_0/l)\,y^2(t_1) \sum_{n=1}^{\infty} \left[(-1)^n (1/A_0)^{n-1}\, n \int_{-s_0}^{0} y^{n-1}(t_2)\,\mathrm{d}s \right] \right\} \right\}. \qquad (9)
\end{aligned}
$$

2.1.2. *Nonlinear application*

Till this point the theory presented is essentially identical to that of Lever & Weaver (1982). We simply utilize the nonlinear, one-dimensional flow equations from the initial formulation of the model rather than linearize these as was done originally. We realize, however, that, for large tube motion, fluid may flow from one flow channel to the next, and the assumption that the tube vibrates in a channel defined by "solid boundaries" may not be valid. We should thus perhaps abandon the existing "unit-cell" concept and determine flow-field variations using two-dimensional fluid mechanics. It must be appreciated that this approach requires formulation of a new theory and we feel that this is beyond the scope of the present study, which is to investigate the role of turbulence in triggering fluidelastic instability, especially since in the vicinity of the fluidelastic stability threshold the tube motion is small (typically less than 2% of a tube diameter). Thus, as an alternative, we examine here a simpler change in the underlying flow redistribution mechanism.

The postulated flow redistribution mechanism, formulated from an analogous transient problem, appears to be well founded for small tube motion. In this case, fluid inertia predominates over viscous effects in a near-wake region (its size is limited by the constrained streamlines, passing along both sides of a tube, as shown schematically in Figure 1) and the resultant time lag is a function of flow velocity only. For increasing tube motion, however, we should perhaps allow also for an unsteady wake effect which may dominate the process of flow separation and redistribution. As shown by Hara (1987), the movement of flow separation points governs the phase relation between the tube motion and flow adjustment. As a result, the time lag increases initially with the amplitude of oscillations and generates destabilizing fluid forces. Approaching the limit cycle, the time lag decreases sharply and, in turn, generates stabilizing fluid forces. The flow redistribution mechanism may thus be both velocity-dependent, due to the perturbation in the free-stream flow for small tube motion, and amplitude-dependent, due to the perturbation in the near wake for large tube motion.

It should be noted that in Hara's experiment the adjacent tubes were free to move and hence produce fluid coupling effects. Nevertheless, we feel that the results may be qualitatively correct also for a single-flexible tube bundle and assume a simple amplitude dependence to express the time lag in the post-stable region. Specifically, we assume that the relevant fluid inertia length decreases linearly with the oscillation amplitude, reducing the time lag in equation (3) from $\tau = l/U_0$ for $y(t) = 0$ (trivial linear solution) to $\tau = 0$ for $y(t) = A_0$ (approximate limit-cycle amplitude). This assumption acts as a "pacemaker" for the underlying instability mechanism and assures the convergence of power-series expansions in equation (9). Also, as shown in our earlier study (Rzentkowski & Lever 1992), it improves the nonlinear predictions of the model substantially by providing the desired nonlinear hardening (in the limit cycle). We realize that at present there is little justification for the assumed amplitude-dependent time lag except that it appears to replicate observed physical behaviour.

2.2. Turbulence Force

To express the turbulence force, we choose here the model of Pettigrew & Gorman (1978). Based on experimental evidence, the authors assume that the power spectral density of the random, homogeneous field of turbulence per unit tube length, $S(f)$, is proportional to the square of the flow dynamic head expressed in terms of the pitch velocity, U_P. That is,

$$S(f) = \left[\frac{1}{2} C_r(f)\rho d U_P^2\right]^2, \tag{10}$$

where ρ is the fluid density and d is the tube diameter. The effective random excitation coefficient, $C_r(f)$, defines the shape of the turbulence spectrum. Because this coefficient is nearly constant in the range of the fundamental frequencies typical for heat exchanger tubes, we use here a flat excitation power spectrum, $C_r(f) = C_r$.

Note that in equation (10), C_r has dimensions of $s^{1/2}$. We eliminate this by introducing a nondimensional excitation coefficient, $C_r' = C_r\sqrt{U_P/fd}$, as suggested by Blevins *et al.* (1981) and Chen & Jendrzejczyk (1987). This nondimensionalization yields the final form of the excitation power spectral density function per unit tube length as

$$S(f) = \left[\frac{1}{2} C_r'\rho (dU_P)^{1.5}\right]^2. \tag{11}$$

We may use equation (11), via inverse Fourier transformation, to generate the turbulence excitation force, $F_T(t)$, in equation (1).

2.3. Fluid-Damping Force

The fluid-damping force is related to the steady-flow drag coefficient, C_D. As suggested by Blevins (1977), the fluid-damping force per unit tube length may be formulated as

$$F_D = \frac{1}{2} C_D \rho d \dot{y}(t) U_0 \ . \tag{12}$$

In general, the fluid damping force is nonlinear. Here, for simplicity, we retain only its linear part, since we observed that the contribution of the higher-order terms to the net system damping is negligible (Rzentkowski & Lever 1992).

3. APPROXIMATE SOLUTION OF EQUATION OF MOTION

The coupled equation of motion, equation (1), cannot be solved analytically in its full nonlinear form. Below, we formulate an approximate method based on superposition of a fluidelastic response with that excited by turbulence.

3.1. Fluidelastic Response

We consider the system subjected to fluidelastic excitation only, $F_T(t) = 0$ in equation (1), and solve the resulting nonlinear equation of motion using the first approximation method of Kryloff & Bogoliuboff (1947). For convenience, we reduce this equation to the basic differential form

$$\ddot{y}(t) + \omega^2 y(t) + F[y(t), \dot{y}(t)] = 0 \ , \tag{13}$$

where, unlike in the original theory of Lever & Weaver, $F[y(t), \dot{y}(t)] = \mu f[y(t), \dot{y}(t)]$ is a nonlinear function of tube displacement and velocity which perturbs the simple linear system oscillating with the frequency $\omega = \sqrt{k/m_0}$ (this frequency differs from ω_0 due to fluidelastic stiffness terms). The constant, μ, is a small positive quantity which defines the size of perturbation, $\mu \ll \omega^2$. After nondimensionalization of equation (13), this condition takes the form

$$\bar{m} \gg 2\left(1 + \frac{s_0}{l}\right)\left(\frac{d}{A_0}\right)\left(\frac{D_E}{d}\right)\left(\frac{U_0}{\omega d}\right)^2 . \tag{14}$$

Provided that condition (14) is satisfied, we can assume the solution of equation (13) to be periodic

$$y(t) = a(t)\cos[\omega t + \Phi(t)] \ , \tag{15}$$

where the amplitude, $a(t)$, and the phase, $\Phi(t)$, are slowly varying functions of time in the state of equilibrium. Their rate of change is given by the following formulae (Kryloff & Bogoliuboff 1947), respectively,

$$\dot{a}(t) = \frac{1}{2\pi\omega} \int_0^{2\pi} F(a\cos\Theta, \ -a\omega\sin\Theta)\sin\Theta \ \mathrm{d}\Theta \ , \tag{16}$$

and

$$\Theta(t) = \omega(a)\,, \tag{17}$$

where $\Theta(t) = \omega t + \Phi(t)$ denotes the total phase and $\omega(a)$ is the amplitude-dependent frequency of oscillation at the limit cycle. This frequency can be expressed as

$$\omega^2(a) = \omega_0^2 + \frac{1}{\pi a}\int_0^{2\pi} F(a\cos\Theta,\ -a\omega\sin\Theta)\cos\Theta\,\mathrm{d}\Theta. \tag{18}$$

For the subsequent analysis, we reduce the nonlinear function $F[\,y(t), \dot{y}(t)]$ to the third order, $n = 2$ in equation (9), and assume a limit cycle of constant amplitude, $\dot{a}(t) = 0$ in equation (16). In this way, we obtain the following nondimensional form of the nonlinear oscillator, representing the solution of equation of motion (1) subjected to fluidelastic excitation only:

$$N\left(\frac{a}{d}\right)^3 + \bar{m}\delta_n\left(\frac{a}{d}\right) = 0, \tag{19}$$

where $\bar{m}\delta_n$ is the net mass-damping parameter and N is the nonlinear fluidelastic term. As we show later in equation (20), the net mass-damping parameter incorporates the positive (structural) and negative (fluidelastic) contributions.

Equation (19) represents the bifurcation formula (Thompson 1982). As illustrated schematically in Figure 2(a), it yields two solution branches, corresponding to the real roots of equation (19): the trivial equilibrium state (linear solution), $a/d = 0$, and the limit cycle (nonlinear solution), $(a/d)^2 = -\bar{m}\delta_n/N$. The trivial equilibrium state is stable for $\bar{m}\delta_n > 0$ (attractor) and unstable for $\bar{m}\delta_n < 0$ (repeller). A dynamic instability arises at the bifurcation point, $\bar{m}\delta_n = 0$. Depending on the sign of the nonlinear term, the solution branches of equation (19) yield two possible theoretical bifurcations: stable for $N > 0$ (solid line) and unstable for $N < 0$ (dashed line). It should be noted that the stable bifurcation represents the soft-excited system. This means that for the linearly unstable system, $\bar{m}\delta_n < 0$, all local motions tend to the stable (attracting) limit cycle. The unstable bifurcation, on the other hand, represents the hard-excited system. This means that the linearly stable system, $\bar{m}\delta_n > 0$, can lose stability if a finite disturbance carries it beyond the unstable (repelling) limit cycle.

At this point, it is instructive to compare the response of a third-order oscillator [Figure 2(a)] with that of a tube bundle [Figure 2(b)]. In our earlier experimental studies (Lever & Rzentkowski 1989, 1993), we have observed that a tube bundle may display hysteresis behaviour; the response jumps at the critical flow velocity for fluidelastic instability ($\bar{m}\delta_n = 0$) for increasing flow, and at a flow velocity lower than critical ($\bar{m}\delta_n > 0$) for decreasing flow. Inside the hysteresis region is a finite domain of attraction bounded by the unstable limit cycle [dashed line in Figure 2(b)]. The hysteresis region diminishes with increasing mass-damping parameter and may disappear at approximately $\bar{m}\delta_0 > 30$ (Lever & Rzentkowski 1993). As depicted in Figure 2, these two types of possible post-stable behaviour of tube bundles, with and without hysteresis, correspond to unstable and stable bifurcations of a third-order oscillator, respectively (the secondary point of bifurcation, which indicates the lower limit of the hysteresis region, cannot be displayed by a simple third-order oscillator). Note that, to allow a direct analogy with a third-order oscillator, we idealize the tube response curves in Figure 2(b) by removing the effect of turbulence

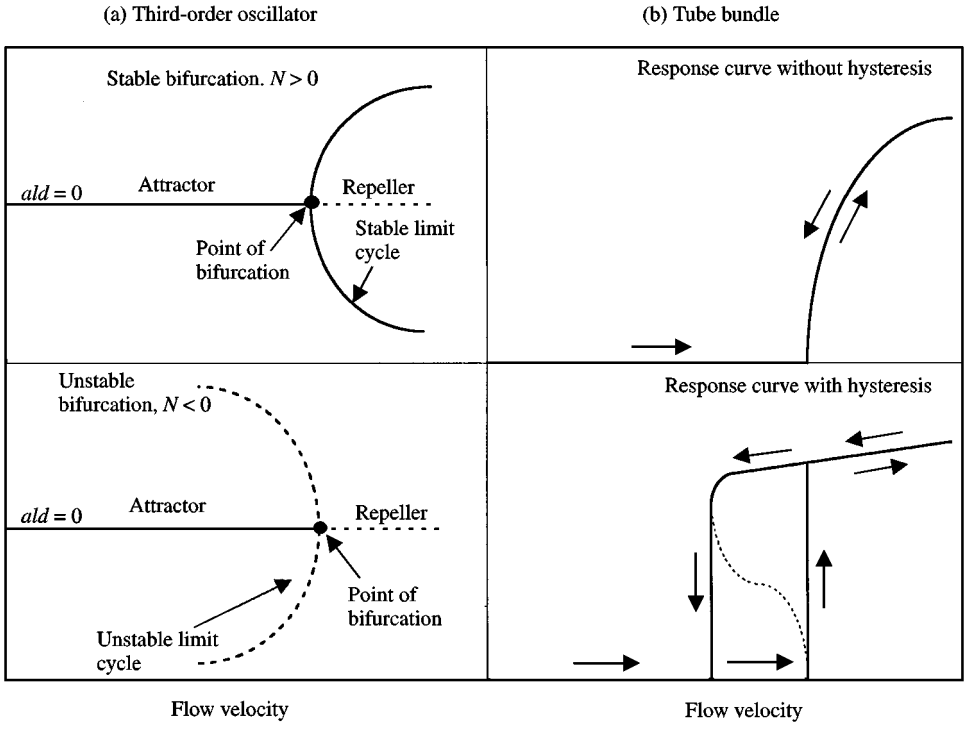

Figure 2. Idealized representation of possible dynamic bifurcations of a third-order oscillator and fluidelastic oscillations of a tube bundle.

buffeting from the overall response. In this way, the equilibrium state for fluidelastic instability becomes trivial.

The trivial equilibrium state of equation (19) is given by the following set of equations which defines the net mass-damping parameter and the oscillation frequency:

$$\bar{m}\delta_n = \bar{m}\delta_0 - 2\pi(D_E/d)\,(d/A_0)\,(s_0/l)^2(s_0/d)^2(1 + s_0/l)\,(\omega/\omega_0)\,U_r^2\{(1 + s_0/l) \times \sin(1/U_r) - (s_0/l)\,(1/U_r)\cos(1/U_r) + h[\sin(1/U_r) + U_r\cos(1/U_r) - U_r]\} - 0{\cdot}5\pi C_D(l/s_0)\,(s_0/d)\,(\omega/\omega_0)\,U_r, \tag{20}$$

and

$$(\omega_0/\omega)^2 = 1 + 2(1/\bar{m})\,(D_E/d)\,(s_0/l)^2(s_0/d)^2(1 + s_0/l)\,(d/A_0)\,U_r^2\{(1 + s_0/l)\,[1 - \cos(1/U_r)] - (s_0/l)\,(1/U_r)\sin(1/U_r) + h[U_r\sin(1/U_r) - \cos(1/U_r)]\}, \tag{21}$$

where $U_r = U_0/\omega l$ denotes reduced flow velocity (ω is the frequency of tube oscillations at a given flow velocity). Note that equation (21) shows explicitly the effect of the fluidelastic stiffness term on the frequency of vibration, ω, via the natural frequency in quiescent fluid, ω_0. For $\omega_0/\omega = 1$, this solution is identical to that obtained by Lever & Weaver (1982).

As discussed already, the nonlinear solution of equation (19) can be written as

$$\frac{a}{d} = \sqrt{-\frac{m\delta_n}{N}}. \tag{22}$$

Equation (22) yields the stable limit cycle for $\bar{m}\delta_n < 0$ and $N > 0$, and the unstable limit cycle for $\bar{m}\delta_n > 0$ and $N < 0$. The nonlinear fluidelastic term, which also defines the size of the limit cycle, is given by

$$\begin{aligned} N = & -2\pi(D_E/d)\,(d/A_0)^3\,(l/s_0)^2\,(s_0/d)^2\,(1 + s_0/l)\,(\omega_0/\omega)\,U_r^2\{\sin(1/U_r)\,[(0{\cdot}75 + s_0/l) \\ & - 0{\cdot}5(1 + s_0/l)\cos(1/U_r)] + 0{\cdot}5(s_0/l)\,(1/U_r)\cos(1/U_r) + h\{\sin(1/U_r)\,[(1{\cdot}5 + s_0/l) \\ & - 0{\cdot}5(1 + s_0/l)\,U_r\sin(1/U_r)] + (1{\cdot}75 + s_0/l)\,U_r[\cos(1/U_r) - 1]\}\} \\ & - 0{\cdot}25\pi C_D(s_0/l)\,(d/s_0)\,(\omega/\omega_0)\,(1/U_r), \end{aligned} \tag{23}$$

with the frequency of oscillations, ω, at a given flow velocity, defined as

$$\begin{aligned} (\omega_0/\omega)^2 = & 1 + 2(1/\bar{m})\,(D_E/d)\,(s_0/l)^2\,(d/s_0)^2\,(1 + s_0/l)\,(d/A_0)^3\,(a/d)^2\,U_r^2\{(A_0/d)^2 \\ & \times (d/a)^2\{(1 + s_0/l)\,[1 - \cos(1/U_r)] - (s_0/l)\,(1/U_r)\sin(1/U_r)\} + 2{\cdot}25(1 + s_0/l) \\ & \times [1 - \cos(1/U_r)] - 0{\cdot}5\sin(1/U_r)\,[(1 + s_0/l)\sin(1/U_r) + (s_0/l)\,(1/U_r)] \\ & + h\{(A_0/d)^2(d/a)^2[U_r\sin(1/U_r) - \cos(1/U_r)] + 0{\cdot}5U_r\sin(1/U_r) \\ & \times [(1 + s_0/l)\cos(1/U_r) + (s_0/l) + 2] - (1{\cdot}5 + s_0/l)\cos(1/U_r)\}\}. \end{aligned} \tag{24}$$

Recall that the nonlinear solution is limited by two conditions: $|y(t)| < A_0$ (clashing boundary) required for the function $F[y(t), \dot{y}(t)]$ to converge, and $\mu \ll \omega^2$ implying that the contribution of nonlinear terms to the final solution is very small. The first condition is always satisfied because of the postulated time lag formulation [$\tau = 0$ for $y(t) = A_0$], while the latter does not pose any restrictions on the derived solution for lightly damped systems ($\delta \leq 0{\cdot}10$, approximately).

3.2. Combined Fluidelastic and Turbulence Response

Having described the fluidelastic response in detail, it is now possible to investigate the effect of turbulence on the underlying instability mechanism.

3.2.1. *Linear response curves*

As follows from random vibration theory, the root-mean-square (r.m.s.) response of a lightly damped, single-degree-of-freedom, linear system to broad band excitation is

$$A_{rms} = \frac{\pi\sqrt{2}}{2}\frac{l_0}{k_0}\sqrt{\frac{S(f_0)\,f_0}{\delta}}, \tag{25}$$

where l_0 is the tube length, f_0 is its natural frequency, k_0 is its structural stiffness coefficient, and δ is its logarithmic decrement of damping. Because both excitation mechanisms are

superimposed, the fluidelastic forces alter the tube stiffness and damping in equation (25). Thus, after substitution of equation (11) into equation (25), the r.m.s. tube response to combined fluidelastic and turbulence excitation takes the nondimensional form

$$\frac{A_{rms}}{d} = \frac{C'_r}{8\pi\sqrt{2}} \left(\frac{U_p}{f_0 d}\right)^{1.5} \frac{1}{\sqrt{\bar{m}(\bar{m}\delta_n)}}, \tag{26}$$

where $\bar{m}\delta_n$ is the net mass-damping parameter. For the linear system under consideration, the net mass-damping parameter is given by the trivial solution of the equation of motion subjected to fluidelastic excitation only, equations (20) and (21). Examination of these equations reveals that the net system damping decreases with flow velocity towards the linear stability threshold, $\bar{m}\delta_n = 0$ in equation (20). Thus, the predicted turbulence response, equation (26), rises asymptotically to infinity. According to this linear model, the location of this asymptote (linear stability threshold) is not affected by turbulence.

3.2.2. *Fluidelastic bifurcation subjected to turbulence*

The linear formulation yields infinite tube response at the stability threshold. In fact, nonlinear fluidelastic forces will limit unstable tube oscillations. To demonstrate this effect, we require a truly nonlinear solution of the equation of motion (1). However, if we conceptually ignore coupling between fluidelastic instability and turbulence buffeting, we may estimate the location of the bifurcation point (nonlinear stability threshold). For this, we superimpose the linear response due to combined excitation, equation (26), to the fluidelastic limit cycle prediction, both of which we may describe analytically. Figure 3 shows graphically this concept.

The stability signalled by stable bifurcation can be qualitatively described by the trivial equilibrium state, $a/d = 0$, since below the point of bifurcation, $\bar{m}\delta_n > 0$ in equation (20), all local motions are asymptotically stable. At the point of stable bifurcation, the nonlinear response is bounded by a limit cycle, while the linear solution becomes infinite. Because these curves do not intersect, the linear stability threshold becomes the lowest stability boundary for the combined system. Therefore, the linear solution is sufficient to establish the dynamic stability criterion for stable bifurcation subjected to turbulence. Nevertheless, various practical measures of the stability threshold rely on the combined response to fluidelastic and turbulence excitation. As we show later, these measures vary with turbulence, even for stable bifurcation.

For unstable bifurcation, the trivial equilibrium state does not guarantee stability below the point of bifurcation, because the stable domain of attraction is bounded by an unstable limit cycle. It follows that, even without nonlinear coupling between fluidelastic and turbulence excitations, the linear response to combined excitation is sufficient to initiate instability below the point of fluidelastic bifurcation when it exceeds the unstable limit cycle. Based on this heuristic approach, the intersection point approximates the actual stability threshold of a tube bundle subjected to combined excitation. We thus expect the dynamic stability criterion for the unstable bifurcation to be sensitive to turbulence buffeting.

We may obtain this intersection point by combining equation (26) with an expression for the unstable limit cycle. For the latter, we may use the third-order solution of equation (1), subjected to fluidelastic excitation only, with the amplitude-dependent time lag between tube motion and flow adjustment, i.e., equation (22) together with equations (23) and (24).

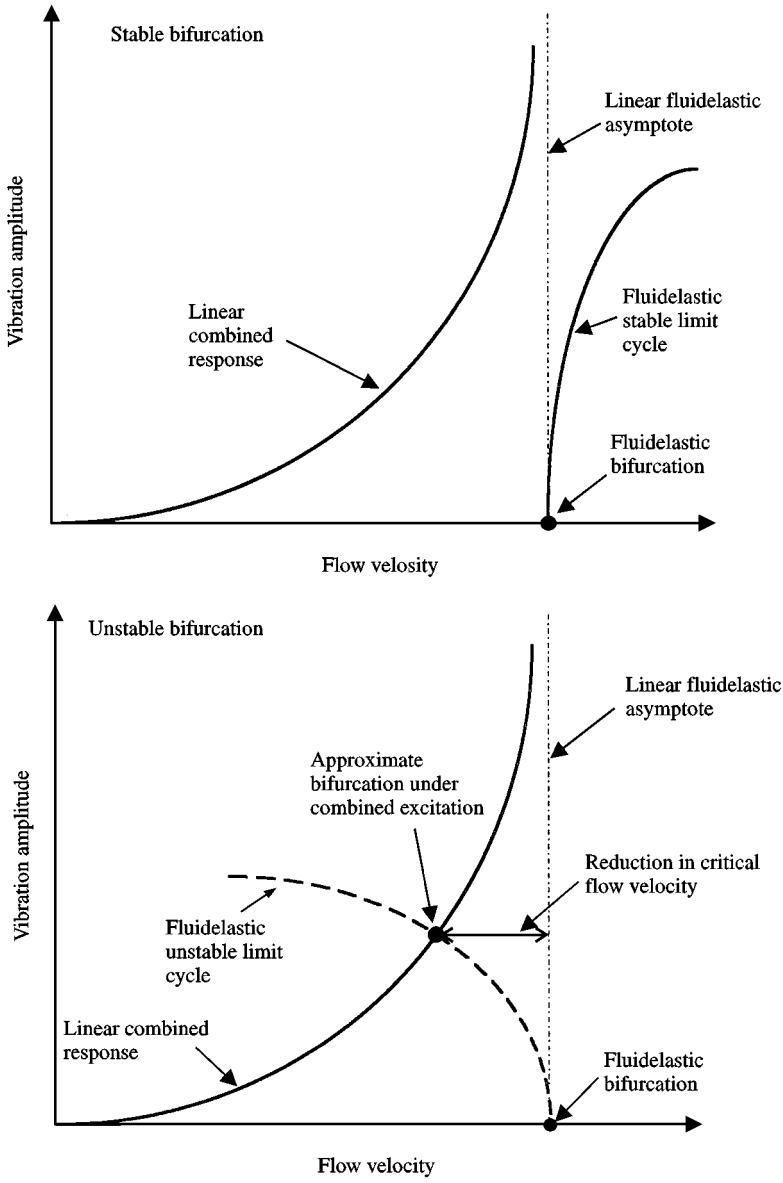

Figure 3. Heuristic representation of linear combined response and fluidelastic bifurcation.

As shown in our earlier study (Rzentkowski & Lever 1992), this solution yields the correct qualitative assessment (stable versus unstable limit cycles) and is very close to a fully nonlinear solution (within 10%) in the vicinity of the stability threshold.

It follows that the approximate stability condition for the nonlinear system, governed by the unstable limit cycle subjected to turbulence, is given by

$$(\bar{m}\delta_n)_{\mathrm{T}} + \left(\frac{1}{8\pi}\, C_r'\right)^2 \left(\frac{U_p}{f_0 d}\right)^3 \frac{N}{\bar{m}(\bar{m}\delta_n)_{\mathrm{NT}}} = 0, \tag{27}$$

where $(\bar{m}\delta_n)_{\mathrm{T}}$ and $(\bar{m}\delta_n)_{\mathrm{NT}}$ represent the trivial and nontrivial solutions of equation (1) subjected to fluidelastic excitation only [respectively, $n = 0$ and $n = 2$ in equation (9)]. The reduced pitch velocity, $U_p/f_0 d$, can be related to U_r by using the following relation:

$$\frac{U_{\mathrm{p}}}{f_0 d} = 2\pi(l/s_0)\,(s_0/d)\,(f/f_0)\,\frac{(A_0/d)}{(T/d)}\,\frac{(P/d)}{(P/d-1)}\,U_r, \tag{28}$$

where the expressions $P/(P-d)$ and $(T-d)/T$ define bundle pitch and pattern, respectively.

Note that if $(\bar{m}\delta_n)_{\mathrm{T}}$ and $(\bar{m}\delta_n)_{\mathrm{NT}}$ were equal (τ independent of tube response amplitude), equation (27) would reduce to

$$\bar{m}\delta_n - \frac{1}{8\pi}\,C_r'\left(\frac{U_P}{f_0 d}\right)^{1\cdot 5}\sqrt{-\frac{N}{\bar{m}}} = 0. \tag{29}$$

As follows from equation (27), the nonlinear term, which reduces the mass-damping parameter at the fluidelastic stability threshold, is directly proportional to the second power of the turbulence excitation strength, C_r', and inversely proportional to the second power of the unstable-limit-cycle amplitude, $\sqrt{-(m\delta_n)_{\mathrm{NT}}/N}$. Note that these variables are mutually dependent. That is, an increase in the turbulence excitation strength results in an increase in the limit-cycle amplitude at the point of intersection between the linear response to combined excitation and the fluidelastic limit cycle.

As formulated, equation (27) defines the approximate reduction in stability threshold that results when tube r.m.s. amplitude exceeds the unstable limit cycle. However, any disturbance that carries the system beyond the unstable limit cycle may cause instability. Since this disturbance arises from turbulence buffeting, the r.m.s. response underestimates its magnitude. We may thus refine this approximation by estimating its actual size: the peak turbulence response expected within some observation period.

For narrow-band, random tube motion excited by turbulence, the displacement peak is governed by the Rayleigh probability-density distribution function (Blevins 1977). Thus, the average number of cycles, N_Y, before this peak exceeds some value, Y, may be shown to be (Lever & Rzentkowski 1989)

$$N_Y(Y) = \mathrm{e}^{(1/2)\,(Y/\sigma)^2}, \tag{30}$$

where σ is the standard deviation. Therefore, for a tube oscillating at frequency f, the average return period in seconds is $T(Y) = N_Y(Y)/f$, and the displacement peak expected in time $T(Y)$ becomes

$$Y = \sigma\sqrt{2\ln[f\,T(Y)]}. \tag{31}$$

We may now modify our heuristic approach to seek the velocity at which the linear response to turbulence exceeds an unstable-limit-cycle amplitude, Y, within an average observation period $T(Y)$. Equation (27) thus becomes

$$(\bar{m}\delta_n)_{\mathrm{T}} + 2\ln[f\,T(Y)]\left(\frac{1}{8\pi}\,C_r'\right)^2\left(\frac{U_P}{f_0 d}\right)^3\frac{N}{\bar{m}(\bar{m}\delta_n)_{\mathrm{NT}}} = 0. \tag{32}$$

4. NUMERICAL SIMULATION

The aforementioned heuristic approach ignores nonlinear coupling between turbulence and fluidelastic excitations. We may include this effect using direct numerical integration of the equation of motion, equation (1). In this method, turbulence can affect tube motion but not *vice versa*. We assume that all motion-dependent fluid forces arise from the "tube-in-channel" theoretical model.

We compute the steady-state, r.m.s. tube response as a function of flow velocity. In this way, we conduct this numerical simulation much as an experimental investigation; the final output is an amplitude versus flow velocity response curve.

4.1. Model Parameters

The numerical model requires certain simulation parameters for its operation. For a chosen integration scheme (fourth-order corrector-predictor) we found that a time step of $\Delta t = T_n/40$ is sufficiently small for accurate and effective simulation. We set the frequency resolution of the turbulence force spectrum, $\Delta f = 2\zeta f_0/K$, based on a consideration of the bandwidth of the tube transfer function in still fluid ($\zeta \approx \delta/2\pi$ is the damping ratio and K is the minimum number of frequency components in the system bandwidth needed to assure accurate turbulence simulations). We can calculate the resolution error by comparing the amplitude of linear resonance under harmonic excitation with the amplitude given by equation (25). For example, for $K = 1$ this error is 25% while $K = 2$ reduces it below 10%. Combined excitation, however, requires practically infinitely small Δf in the immediate vicinity of the stability threshold. Thus, we choose $K = 10$ for the lowest damping case examined here, $\delta = 0{\cdot}01$, and use the resulting Δf for all subsequent simulations.

Having selected the time and frequency steps, we calculate the maximum frequency in the turbulence force spectrum using the Nyquist criterion, $F_{\max} = 1/2\Delta t$. The length of the corresponding time series of the turbulence force thus is $T_{\max} = 1/\Delta f$. If required, we conduct simulations of arbitrary length, without the time-consuming computation associated with the use of a very long inverse fourier transformation, by piecing together turbulence-force time series of $T_{\max}$ length. We carefully checked this technique against the use of one very long, unique time series and found it to yield equivalent results.

We express the random nature of the turbulence force by assigning random phases to each frequency component in the inverse fourier transformation (each set of phases produces a different turbulence force time series). We found that the steady-state tube response is essentially independent of this randomizing effect, especially if Δf is small compared with the bandwidth of the transfer function. For example, the maximum discrepancy in computed tube response resulting from random phase selections is within 5% for $K = 2$ and 0·2% for $K = 80$. Therefore, we use only one set of random phases to reduce computational effort.

4.2. Model Operation

Figure 4 shows a flow chart for the operation of the coupled model. First, we select the numerical parameters defining the bundle and flow conditions, together with the simulation parameters, such as time step and length of simulation. At each flow velocity we then generate the turbulence force time series from the spectrum, equation (11), using the inverse

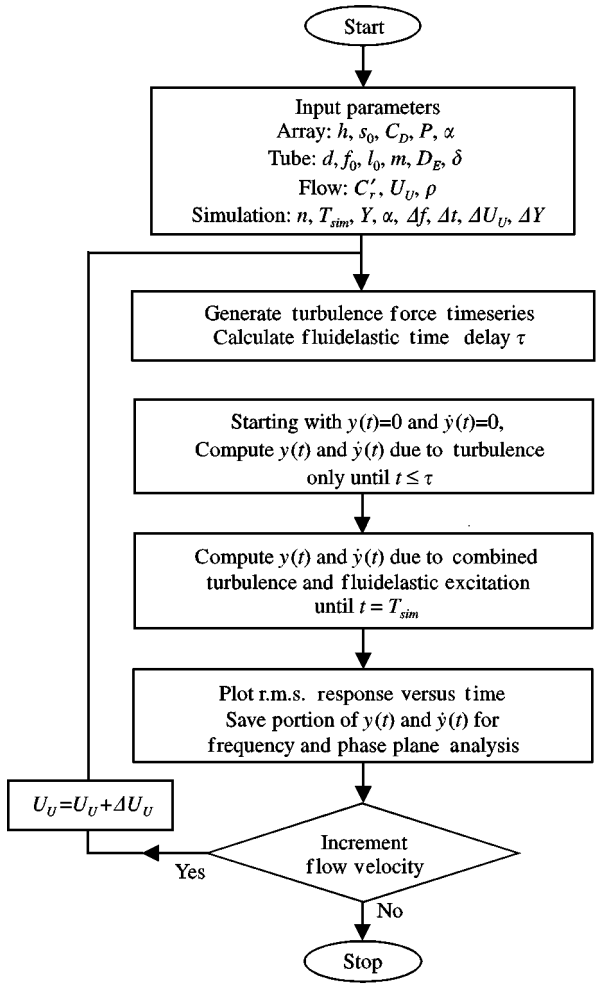

Figure 4. Flowchart for numerical simulation.

Fourier transformation. Next, we calculate the fluidelastic streamtube velocity and time lag. At this point, the simulation begins with zero initial tube displacement and velocity. We initially compute the response to turbulence only, using the central difference method as a starting procedure. At time $t = \tau$ it becomes possible to calculate the fluidelastic excitation force. The simulation proceeds, for the prechosen length of time (typically 30 min of tube response), with the r.m.s. tube displacement computed and saved at each time step. We examine the results for a given flow velocity and, if desired, increment it and repeat the procedure.

We observed that, for a lightly damped system very near the stability threshold, the simulation transient time can be extremely long, exceeding 30 min of tube response. Therefore, to perform the simulations near the stability threshold without the prohibitively long computations, we use the approximate steady-state response value, given by equation (26), as an initial parameter.

5. RESULTS

Below, we present the theoretical results obtained with this model for two arrays also studied experimentally by the authors in 1993: a parallel triangular array of pitch ratio 1·375 and a square array of pitch ratio 1·433. The array parameters are thus expressed in terms of the physical quantities, describing the tested configurations. As with the experimental investigation, the tube parameters are $d = 60\,\text{mm}$, $f_0 = 5{\cdot}0\,\text{Hz}$ and $\delta = 0{\cdot}01$ (here, we also use $\delta = 0{\cdot}10$). The fluid density is $\rho = 1{\cdot}22\,\text{kg/m}^3$. For the parallel triangular array, the random excitation coefficient, which we obtained through direct measurement (Rzentkowski 1991) is $C_r' = 0{\cdot}065 \pm 10\%$. This agrees reasonably well with the value of $C_r = 0{\cdot}012\ \text{s}^{1/2}$ reported by Pettigrew & Gorman (1978). For the square array, we measured $C_r' = 0{\cdot}200 \pm 10\%$. Table 1 summarizes all nondimensional parameters required by the model, together with the empirical coefficients.

5.1. Linear Response Curves

An early paper by the authors (Lever & Rzentkowski 1989) discussed in detail the theoretical, linear response to combined turbulence and fluidelastic excitations. Here, we present a few key results because they also demonstrate tube response to turbulence for a stable fluidelastic bifurcation.

Figure 5 shows a set of linear, theoretical response curves for a parallel triangular array. We set the mass-damping parameter at $\bar{m}\delta_0 = 10$ ($\delta = 0{\cdot}01$ and $\delta = 0{\cdot}10$) and use a range of the random excitation coefficient, $C_r' = 0{\cdot}065$, $0{\cdot}100$ and $0{\cdot}130$, holding the plotting scale fixed. To facilitate a direct comparison, we also normalize the flow velocity with respect to the critical for fluidelastic instability (as we discuss later, the critical flow velocities depend on damping due to the fluidelastic stiffness effect which alters the frequency of tube oscillation at the stability threshold, i.e., $U_P/f_0 d = 7{\cdot}86$ for $\delta = 0{\cdot}01$ and $U_P/f_0 d = 7{\cdot}68$ for $\delta = 0{\cdot}10$). It can be seen that all curves show a smooth increase in r.m.s. response towards a vertical asymptote at the critical flow velocity (the normalized flow velocity of 1·0). The rate of increase depends on the random excitation coefficient used. In experimental situations, however, the stability boundary is not known and its location must be assigned based on one of the commonly used definitions: such as (i) an abrupt change in slope of the response curve, (ii) an amplitude exceedence level, or (iii) an intersection with the velocity axis of the steepest tangent to the response curve. As demonstrated in Figure 5, an increase in turbulence reduces the apparent fluidelastic stability threshold, whichever definition is used (here, as an example, we showed the fixed-amplitude criterion of 0·2% of tube diameter). Note that, for constant $\bar{m}\delta_0$, an increase in damping has a similar effect since, as follows from equation (26), the heavier-damped tube (lower $\bar{m}$) shows larger turbulence

Table 1
The nondimensional parameters and coefficients required by the model

Array geometry	T/d	A_0/d	s_0/d	D_E/d	l/s_0	C_r'	h	C_D
Parallel triangular	$(P/d)\cos\alpha$	$(P/d) - 1$	$(P/d)\alpha$	$(d/P)\alpha$	—	—	—	$2(A_0/d)h$
$\alpha = \pi/6$, $P/d = 1{\cdot}375$	1·191	0·375	0·720	0·381	4·0	0·065	0·30	0·225
Square	P/d	$(P/d) - 1$	P/d	$\alpha/8$	—	—	—	$2(A_0/d)h$
$\alpha = \pi/2$, $P/d = 1{\cdot}433$	1·433	0·433	1·433	0·196	4·0	0·200	0·35	0·300

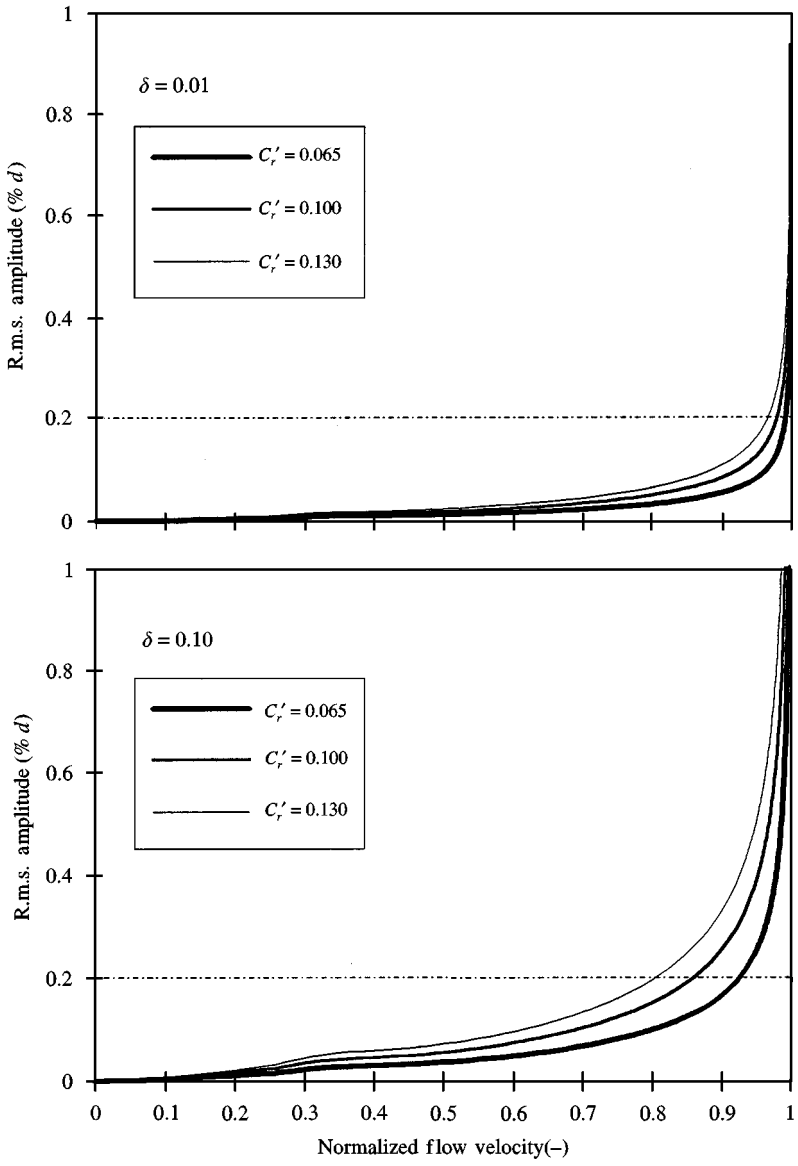

Figure 5. Theoretical linear response curves to combined excitation for $\bar{m}\delta_0 = 10$ (here, flow velocity is normalized by the critical).

response. This effect can lead to the influence of experimentally observed separation of $\bar{m}$ and δ on the stability threshold (Lever & Rzentkowski 1989). Nevertheless, it appears that this is entirely due to the way turbulence affects our interpretation of the response curves; the linear fluidelastic stability threshold is unaffected by turbulence.

Table 2 compares the linear, steady-state, numerical simulation results for separate turbulence buffeting and combined excitation with the corresponding analytical solutions ($C_r' = 0{\cdot}065$, simulation time of 30 min). For $\delta = 0{\cdot}01$, the turbulence r.m.s. response agrees

TABLE 2
Comparison of analytical and numerical r.m.s. tube response for the linear solution for $(\bar{m}\delta)_0 = 10$

Normalized flow velocity	Damping δ	Analytical solution (% d)		Numerical solution (% d)	
		Turbulent	Combined	Turbulent	Combined
0·70	0·01	0·0236	0·0218	0·0237	0·0229
0·80	0·01	0·0288	0·0321	0·0289	0·0340
0·90	0·01	0·0344	0·0539	0·0344	0·0561
0·99	0·01	0·0396	0·1941	0·0396	0·1345
1·01	0·01	0·0408	Unstable	0·0408	Unstable
0·70	0·10	0·0721	0·0664	0·0712	0·0669
0·80	0·10	0·0880	0·0978	0·0867	0·0976
0·90	0·10	0·1051	0·1652	0·1033	0·1624
0·99	0·10	0·1211	0·5835	0·1189	0·6009
1·01	0·10	0·1249	Unstable	0·1226	Unstable

to better than 0·5% while the combined r.m.s. response agrees to better than 5·0% at each velocity point except very near the stability threshold (the simulation error in the threshold estimation, resulting from the fluidelastic excitation only, is 0·06%). Just below the stability threshold, the simulated tube response is extremely sensitive to the details of the turbulence time series used. This is because of an increasing discretization error associated with the decreasing bandwidth of the system. For $\delta = 0{\cdot}10$, the discretization error is not so apparent. It can be seen that the turbulence r.m.s. response agrees to better than 2·0%, while the combined r.m.s. response agrees to better than 3·0% at each velocity point (the simulation error in the threshold estimation is 0·03%).

These simulation errors are certainly well within the uncertainty of experimental data. Beside, some variations in the simulated response are unavoidable since we generated specific time series of finite length, whereas equation (26) applies, strictly speaking, to infinitely long records. Therefore, we feel that the numerical simulation of combined fluidelastic and turbulence excitation (at least in linear form) yields reasonable results.

5.2. FLUIDELASTIC BIFURCATION SUBJECTED TO TURBULENCE

Our main interest in examining nonlinear tube response to combined excitation is to determine the effect of turbulence on the practical stability threshold. As shown in Figure 3, this analysis requires limit-cycle prediction. We may expect that, to a certain degree, limit-cycle amplitudes are also affected by turbulence. As shown by Zhu & Yu (1986), a limit-cycle amplitude of a self-excited system (Van der Pol oscillator was used by the authors) subjected to random perturbation decreases initially and then increases with increasing perturbation intensity. Nevertheless, we do not investigate this effect in detail here and use only one value of the random excitation coefficient for subsequent numerical simulations.

5.2.1. *Fluidelastic limit cycles*

We may calculate the fluidelastic limit cycles from equation (22), together with equations (20), (23) and (24). For the two arrays of interest, Figure 6 shows the predicted amplitudes

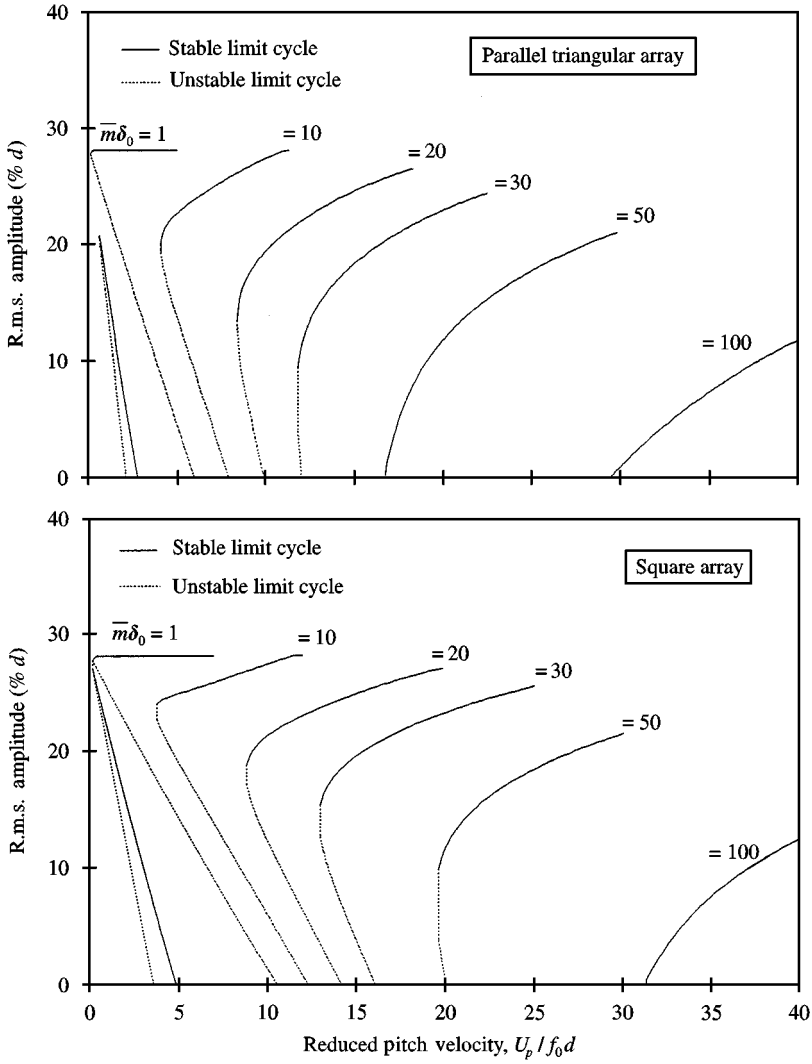

Figure 6. Analytically predicted, third-order limit cycle oscillations.

for a variety of mass-damping parameters: $\bar{m}\delta_0 = 1,\ 10, 20, 30, 50$ and 100 with $\delta = 0{\cdot}01$ (note that the separation in $\bar{m}$ and δ does not have a direct effect on limit-cycle amplitudes; it affects only oscillation frequency). For a parallel triangular array, the model predicts unstable limit cycles followed by stable limit cycles (unstable bifurcation) below $\bar{m}\delta_0 \approx 30$. In the higher mass-damping parameter range, the model predicts only stable limit cycles (stable bifurcation); the rate of increase of limit-cycle amplitudes becomes lower with increasing $\bar{m}\delta_0$. For a square array, we found essentially similar results: an unstable bifurcation below $\bar{m}\delta_0 \approx 50$ and a stable bifurcation in the higher mass-damping parameter range. In both cases, the model predicts the multiple response branches at $\bar{m}\delta_0 = 1$ which, as we discuss later in some detail, are due to the existence of several stability boundaries in the region of low mass-damping parameters. Here, for clarity, we show only two upper response branches which consist of stable and unstable limit cycles.

It is interesting to note that the contribution of fluidelastic stiffness terms to the final solution is more pronounced at the stability threshold than at the limit cycle. For both arrays investigated here, the frequency of tube oscillation at the stability threshold is reduced by approximately 2·5% for $\bar{m}\delta_0 = 1$ and 0·05% for $\bar{m}\delta_0 = 100$. This effect increases with damping [lower $\bar{m}$ in equation (24)]. For example, for $\delta = 0{\cdot}10$ the frequency reduction at the stability threshold is approximately 25% for $\bar{m}\delta_0 = 1$ and 0·5% for $\bar{m}\delta_0 = 100$. The main significance of this frequency reduction is to affect the reduced critical velocity, $U_P/f_0 d$, and to lead to the influence of experimentally observed separation of $\bar{m}$ and δ on the stability threshold (Lever & Rzentkowski 1989). Similar results were reported by Price & Païdoussis (1984) for their semi-empirical dynamic model which is also based on the motion of a single flexible tube.

Figure 7 compares the analytical and numerical solutions of the equation of motion (1) for a parallel triangular array. To generate the numerical results, we harmonically excited the tube in the vicinity of the limit cycle and carefully examined the response record (10 min of tube response) by checking for an exponential increase or decrease of the oscillation envelope. A constant-amplitude sine wave signalled a limit cycle: either stable, attracting all local motions (convergence of numerical solution onto a limit cycle) for flow velocities higher than critical for fluidelastic instability, or unstable, repelling all local motions (divergence of numerical solution from a limit cycle) for flow velocities lower than critical for fluidelastic instability. In the latter case, all local motions in the vicinity of the limit cycle diverged from the limit cycle, either towards the trivial equilibrium solution, $a/d = 0$, for the amplitude of initial disturbance lower than that of the limit cycle, or towards infinity for the amplitude of initial disturbance higher than that of the limit cycle. Thus, at a given flow velocity, we incremented or decremented the amplitude of initial disturbance in small steps till the transition in the stability of numerical solution (neither decay nor growth) was found. We used the amplitude of the initial disturbance, for which the constant-amplitude sine wave was observed, to numerically assess the unstable limit-cycle amplitude. We conducted two separate sets of numerical simulations: first at $\bar{m}\delta_0 = 10$ for the unstable bifurcation and second at $\bar{m}\delta_0 = 100$ for the stable bifurcation. As indicated in Figure 7, in both cases investigated (stable and unstable bifurcations), we found a very good agreement between the third-order analytical solution, equation (22), and the corresponding numerical simulation. The predicted limit-cycle amplitudes are qualitatively identical (stable versus unstable) and agree to better than 10% at each velocity point. The discrepancy between these solutions is less at the lower limit-cycle amplitudes near the bifurcation point.

Figure 8 shows experimental response curves obtained by the authors (Rzentkowski & Lever 1992). It can be seen that, for these same two arrays (each with a single, transverse-to-flow degree-of-freedom), the nonlinear predictions of the model presented previously in Figure 6, agree well qualitatively with experiment. We found broad hysteresis (i.e., unstable limit cycles followed by stable limit cycles at larger amplitudes) in the low mass-damping parameter range. The observed hysteresis regions diminish with increasing mass-damping parameter and disappear for $\bar{m}\delta_0 > 30$. Maximum amplitudes decrease with increasing mass-damping parameter and do not exceed $0{\cdot}3d$ for either array. The model yields very similar results.

5.2.2. *Nonlinear response curves*

As follows from our heuristic approach (see Figure 3), the interaction mechanism between fluidelastic excitation and turbulence is dependent on the tube nonlinear

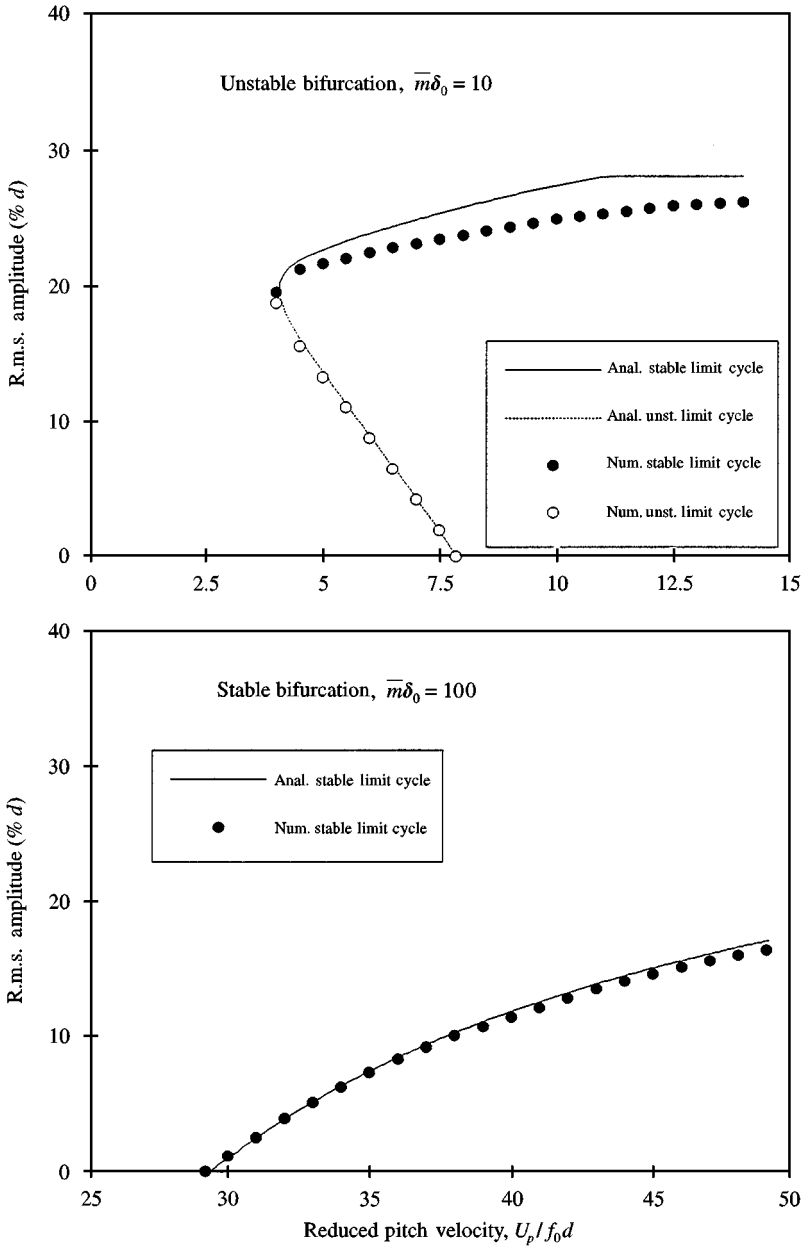

Figure 7. Comparison between analytically predicted and numerically calculated third-order limit cycle oscillations for unstable ($\bar{m}\delta_0 = 10$) and stable ($\bar{m}\delta_0 = 100$) bifurcations.

characteristics: stable and unstable bifurcations. Because both types of behaviour are predicted by the underlying model (see Figure 6), we can use it to assess qualitatively the effect of turbulence on the fluidelastic stability threshold. We conducted two separate sets of numerical simulations for a parallel triangular array: first at $\bar{m}\delta_0 = 10$ for the unstable bifurcation and second at $\bar{m}\delta_0 = 100$ for the stable bifurcation, using the baseline value of

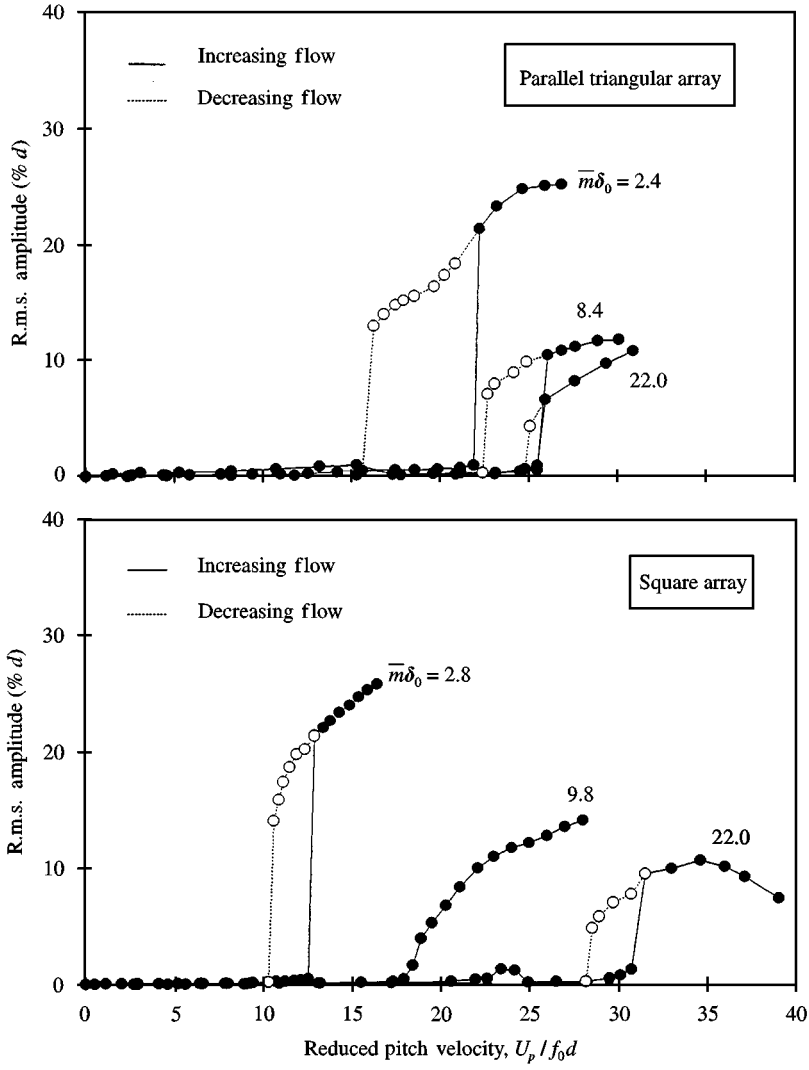

Figure 8. Experimental response curves for single-degree-of-freedom tube bundles (Rzentkowski & Lever 1992).

the random excitation coefficient, $C'_r = 0{\cdot}065$. Because of excessive computational effort near the stability threshold, we conducted this analysis with $\delta = 0{\cdot}10$ to reduce the transient time. In each set of simulations, we compared the simulated, nonlinear tube response to the analytical expressions for linear asymptote, equation (20), and to the fluidelastic limit cycle, equation (22).

As shown in Figure 9, the simulated response curves display the expected behaviour. For the unstable bifurcation, the system experiences a sudden response jump, triggered by turbulence, to unstable oscillations (limit cycle) at a flow velocity lower than the linear asymptote. Thus, the numerical simulation confirms that the linear threshold is unconservative. For the stable bifurcation, the system response remains stable for flow velocities

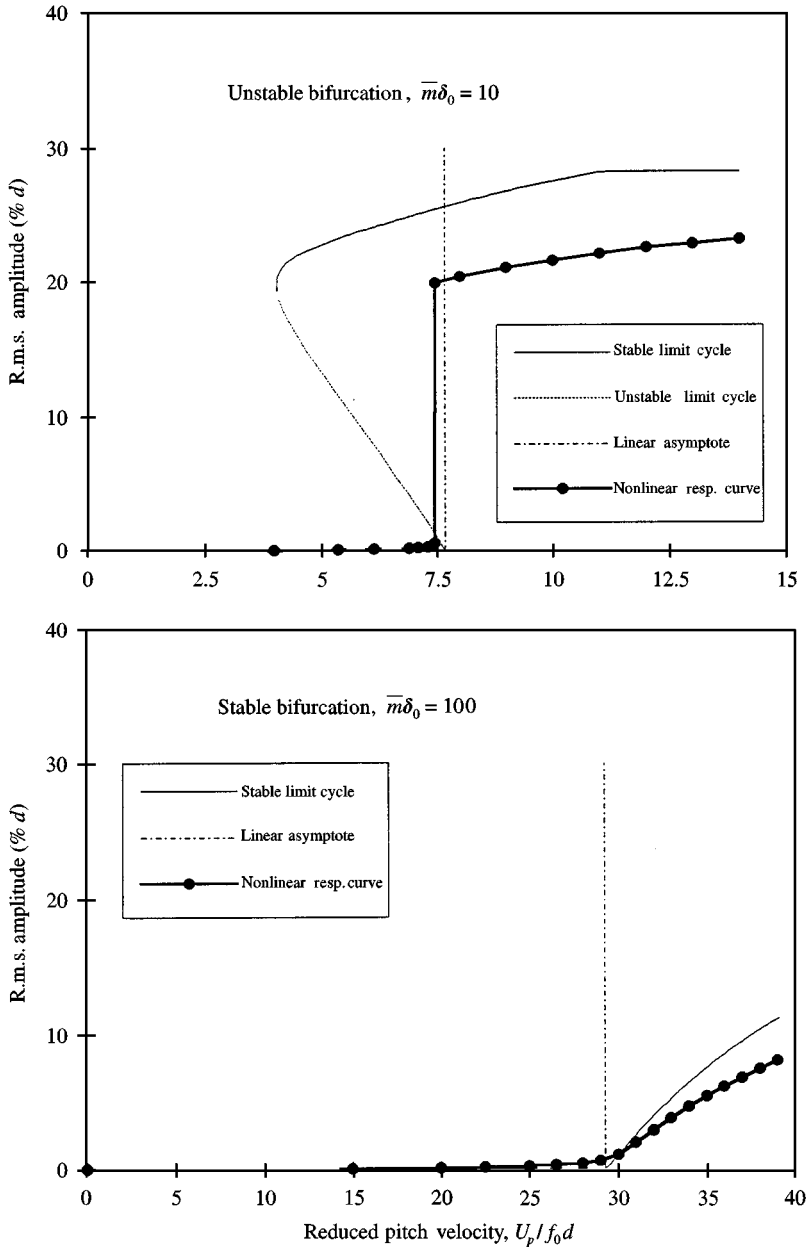

Figure 9. Numerical nonlinear response curves to combined excitation ($C_r' = 0{\cdot}065$) for unstable ($\bar{m}\delta_0 = 10$) and stable ($\bar{m}\delta_0 = 100$) bifurcations. Here, also shown are linear and nonlinear fluidelastic predictions.

lower than critical, and then follows the analytically predicted limit cycle in the post-stable region. This suggests that the linear asymptote becomes the lowest stability boundary for the combined system (this is in agreement with the concept presented in Figure 3). As discussed in Section 5.1, turbulence does affect our interpretation of response curves.

TABLE 3
Turbulence sensitivity of the unstable bifurcation for $\bar{m}\delta_0 = 10$ and $\delta = 0{\cdot}10$: comparison between the numerical and analytical solutions; $T(Y) = 10\,\text{min}$, C'_r varied

Array geometry	C'_r	Critical flow velocity, $U_P/f_0 d$		Threshold reduction (%)	
		Numerical	Equation (18)	Numerical	Equation (18)
Parallel triangular	0·000	7·68	7·68	—	—
	0·065	7·44	7·45	3·1	3·0
	0·130	7·31	7·32	4·8	4·7
Square	0·000	11·70	11·70	—	—
	0·200	10·64	10·64	9·1	9·1
	0·400	10·08	10·09	13·9	13·8

Specifically, an increase in turbulence response leads to an apparent decrease in the critical velocity assigned on the basis of standard threshold definitions (see Figure 5). Also, turbulence appears to reduce the amplitude of the post-stable limit cycles for both stable and unstable bifurcations.

For the unstable bifurcation, the simulated response curve shows a lowering of the stability threshold, as predicted by the analytical superposition approach [equation (31)]. To examine this effect more closely and to validate equation (31), we conducted a separate series of simulations for a parallel triangular and a square array. We varied the random excitation coefficient to demonstrate the effect of increasing turbulence on the stability threshold. Table 3 presents the analytical and numerical results for $\bar{m}\delta_0 = 10$. To generate the analytical results, we set the average return period at $T(Y) = 10\,\text{min}$ (typically used during experimental investigations to allow tube motion to stabilize at a given flow velocity). Thus, for a direct comparison with the analytical results, the simulation running time, after reaching steady-state response level, was also 10 min. For the baseline value of the random excitation coefficient, the resultant threshold reduction is 3.1% for a parallel triangular array and 9.1% for a square array. These are almost identical values to those predicted by the analytical solution. Note that these results also show the correct qualitative effect; the threshold reduction increases with the turbulence strength, C'_r.

We also examined the role of unstable-limit-cycle amplitude on the threshold reduction caused by turbulence. For this, we varied the nonlinear fluidelastic parameter, N, in equation (31); we calculated this coefficient from equation (23) and increased it by a factor of four [as follows from equation (22), this is equivalent of halving the unstable-limit-cycle amplitude]. For the baseline value of the random excitation coefficient, these results are shown in Table 4. Here, we also increased the tube average return period to $T(Y) = 1$ year to model the long-term operation of steam generators or heat exchangers. It can be seen that the resultant threshold reduction may reach 10% for a parallel triangular array and 20% for a square array, approaching the size of the experimentally observed hysteresis region.

5.2.3. *Stability map*

For the model examined here, the analytical prediction [equation (31)], which we derived by ignoring coupling between turbulence and fluidelastic excitations, agrees very well with

TABLE 4
Turbulence sensitivity of the unstable bifurcation for $\bar{m}\delta_0 = 10$ and $\delta = 0{\cdot}10$: $T(Y) = 1$ yr, N (unstable-limit-cycle amplitude) varied

Array geometry	Nonlinear coefficient N	Critical flow velocity $U_P/f_0 d$	Threshold Reduction (%)
Parallel triangular	0	7·68	—
	Baseline, equation (11)	7·39	3·8
	4 × baseline	7·21	6·1
Square	0	11·70	—
	Baseline, equation (11)	10·32	11·8
	4 × baseline	9·63	17·7

the numerical simulation. Thus, the stability condition for a randomly oscillating tube subjected to the fluidelastic excitation can be approximately expressed as

$$(\bar{m}\delta_n)_{\mathrm{T}} + 2\ln[fT(Y)]\left(\frac{1}{8\pi}\,C_r'\right)^2\left(\frac{U_P}{f_0 d}\right)^3 \frac{N}{\bar{m}(\bar{m}\delta_n)_{\mathrm{NT}}} = 0 \quad \text{for } N < 0,$$
$$(\bar{m}\delta_n)_{\mathrm{T}} = 0 \quad \text{for } N \geq 0, \tag{32}$$

where $(\bar{m}\delta_n)_{\mathrm{T}}$ and $(\bar{m}\delta_n)_{\mathrm{NT}}$ represent, respectively, the trivial and nontrivial form of equation (20), and the nonlinear fluidelastic term N is given by equations (23) and (24).

Figure 10 shows the numerical solution of equation (32), together with the fluidelastic prediction only [linear stability curve, $(\bar{m}\delta_n)_{\mathrm{T}} = 0$], in the form of a stability map for a parallel triangular and a square array examined above ($\delta = 0{\cdot}10$), using the baseline value of the random excitation coefficient and $T(Y) = 10$ min. Especially for the square array, this analysis suggests that the effect of superposition of turbulence on fluidelastic stability threshold cannot be ignored. Note also that the multiple stability boundaries at low mass-damping parameters, resulting from the time delay between tube motion and the associated fluid forces, are absorbed by the interaction between turbulence and unstable limit cycles.

6. DISCUSSION

The trends predicted by the nonlinear model agree with our interpretation of the interaction between turbulence and fluidelastic excitation, as depicted in Figure 3. Nevertheless, uncertainty exists in the quantitative results. In particular, experiments indicate that unstable-limit-cycle amplitudes may be much lower than those predicted here (Lever & Rzentkowski 1993). This makes the array much more susceptible to turbulence-triggered instability. Also, the turbulence field in actual steam generators or heat exchangers may not be uniform, so C_r' may vary with location. Thus, the authors caution against using this model as a design tool.

Nevertheless, our study shows that turbulence can clearly trigger fluidelastic instability for the case of unstable bifurcation. This suggests that a conservative design approach is appropriate, i.e., the lower limit of hysteresis should be used as the practical fluidelastic stability threshold (this will also prevent any transient excitation of fluidelastic instability).

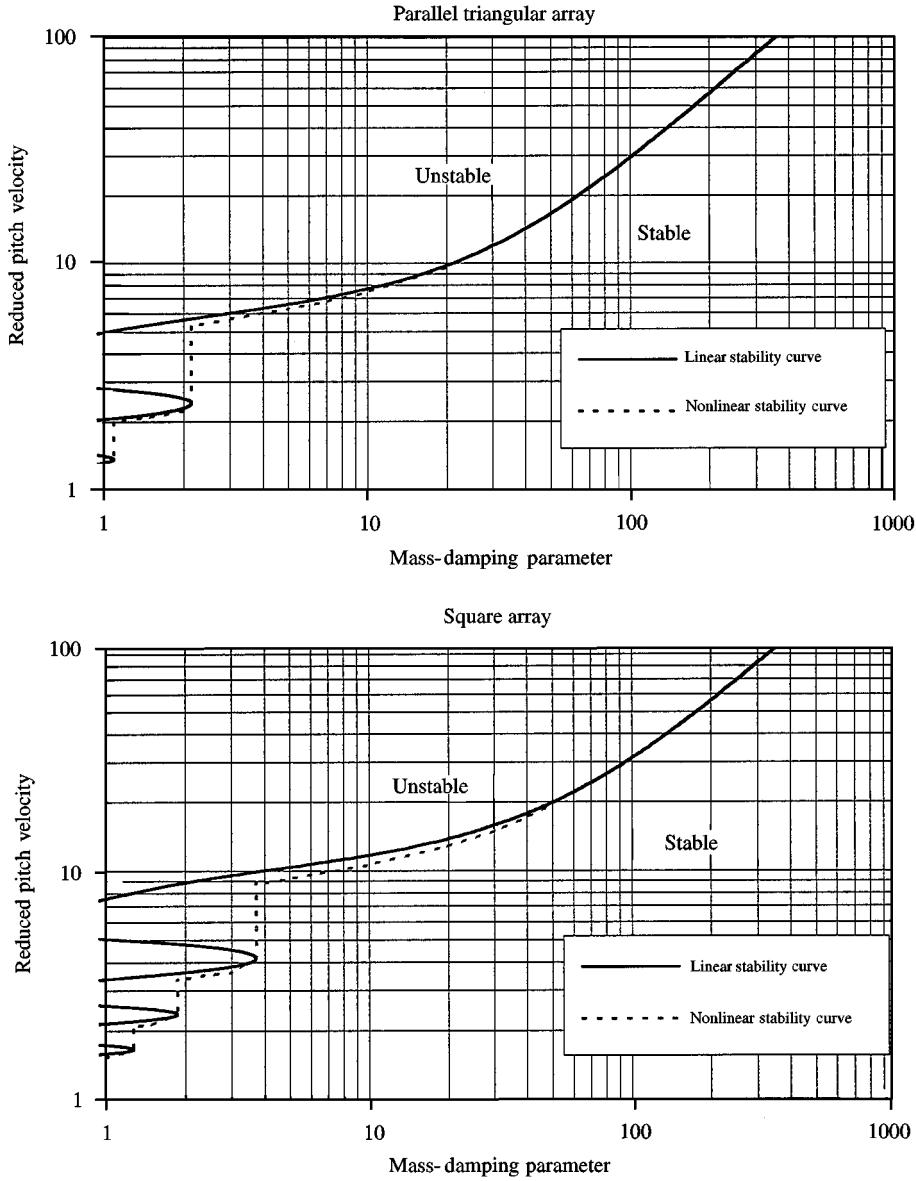

Figure 10. Theoretical stability curves ($\delta = 0{\cdot}10$) showing the effect of turbulence on the fluidelastic stability threshold for a parallel triangular and a square array: $C'_r = 0{\cdot}065$ and $C'_r = 0{\cdot}200$, respectively. The possible peak size of turbulence buffeting is calculated using $T(Y) = 10$ min.

7. CONCLUSIONS AND RECOMMENDATIONS

We have conducted a theoretical study to examine the effect of turbulence on fluidelastic instability in tube bundles. The study was focused on the simplest physical system while retaining the behaviour of full bundles. The fluidelastic model was thus conceptually idealized to represent the tube as a simple, third-order fluidelastic oscillator subjected to

turbulence excitation. Although the model is oversimplified on the basis of the underlying fluid mechanics, it gives the correct qualitative assessment of the post-stable behaviour of a tube bundle and provides physical insight into the role of turbulence in triggering fluidelastic instability. Here, we investigated stable and unstable bifurcations because both types of behaviour have been observed experimentally and were also predicted by the fluidelastic model. Based on theoretical considerations and a series of numerical simulations, we derived an approximate stability condition for a randomly oscillating tube subjected to fluidelastic excitation. This leads to some general conclusions regarding the role of turbulence in prediction of fluidelastic instability.

(a) For stable bifurcation (no hysteresis) linear theory yields the lowest stability threshold. In this case, the fluidelastic stability boundary cannot be reduced by interaction with turbulence. However, the response to turbulence below the threshold can shift the practical stability threshold assigned on the basis of commonly used definitions. For most of them, increasing response to turbulence decreases the apparent stability threshold.
(b) For unstable bifurcation (hysteresis) a nonlinear theory is required for stability analysis. In this case, interaction with turbulence lowers the fluidelastic stability boundary. The threshold reduction increases with turbulence excitation strength and decreases with unstable-limit-cycle amplitude. For long-term operation, this reduction may approach the size of the hysteresis region. That is, the lower limit of the hysteresis region is the practical stability threshold for equipment design.

The threshold reduction, based on superposition of the linear response to turbulence with the third-order fluidelastic limit cycle, agrees well with fully nonlinear numerical results (direct integration of the equation of motion). This provides a simple way of examining the role of turbulence in reducing the fluidelastic stability threshold and it may be applicable to other nonlinear fluidelastic models. It has to be remembered, however, that idealizations have been made here to formulate this heuristic analysis. Consequently, considerable scope for further work exists, as follows.

(i) The existing "unit-cell" concept may not be valid for large tube motion. Consideration should be given to utilize two-dimensional fluid mechanics to formulate a better nonlinear model for fluidelastic instability in tube bundles. In view of the present level of effort, however, this may be very challenging.
(ii) The postulated flow redistribution mechanism, which accounts for most of the modeled characteristics of fluidelastic instability, requires experimental validation. Particularly important is the determination of the velocity and amplitude dependence of the assumed phase lag. Unfortunately, these experiments are rather difficult to perform due to the high level of turbulence generated by tube bundles.

ACKNOWLEDGEMENT

The authors gratefully acknowledge the financial support of the Natural Sciences and Engineering Research Council of Canada, and the CANDU Owners Group.

References

Blevins, R. D. 1977 *Flow-Induced Vibration.* New York: Van Nostrand Reinhold.
Blevins, R. D., Gilbert, R. J. & Villard, B. 1981 Experiments on vibration of heat exchanger tube arrays in cross flow. In *Proceedings SMiRT 6th International Conference on Structural Mechanics in Reactor Technology*, Paris, Paper B6/9.

Chen, S. S. & Jendrzejczyk, J. A. 1981 Experiments on fluidelastic instability in tube banks subjected to liquid cross flow. *Journal of Sound and Vibration* **78,** 355–381.

Chen, S. S. 1984 Guidelines for the instability flow velocity of tube arrays in cross-flow. *Journal of Sound and Vibration* **93,** 439–455.

Chen, S. S. & Jendrzejczyk, J. A. 1987 Fluid excitation forces acting on a square tube array. *ASME Journal Fluids Engineering* **109,** 415–423.

Franklin, R. E. & Soper, B. M. H. 1977 An investigation of fluidelastic instabilities in tube banks subjected to fluid cross flow. In *Proceedings 4th International Conference on Structural Mechanics in Reactor Technology*, San Francisco, Paper F6/7, 1–14.

Hara, F. 1987 Unsteady fluid dynamic forces acting on a single row of cylinders vibrating in cross flow. In *Flow-Induced Vibration* 1987, PVP-Vol. 112, pp. 51–58. New York: ASME

Kryloff, N. & Bogoliuboff, N. 1947 *Introduction to Nonlinear Mechanics.* Princeton: Princeton University Press.

Lever, J. H. & Weaver, D. S. 1982 A theoretical model for fluidelastic instability in heat exchanger tube bundles. *ASME Journal of Pressure Vessel Technology* **104,** 147–158.

Lever, J. H. & Rzentkowski, G. 1989 Determination of the fluidelastic stability threshold in the presence of turbulence: a theoretical study. *ASME Journal of Pressure Vessel Technology* **111,** 407–419.

Lever, J. H. & Rzentkowski, G. 1989 An investigation into the post-stable behavior of a tube array in cross-flow. *ASME Journal of Pressure Vessel Technology* **111,** 457–465.

Lever, J. H. & Rzentkowski, G. 1993 Dependence of post-stable fluidelastic behavior on the degrees of freedom of a tube bundle. *Journal of Fluids and Structures* **7,** 471–496.

Païdoussis, M. P. 1983 A review of flow-induced vibration in reactor and reactor components. *Nuclear Engineering and Design* **74,** 31–60.

Pettigrew, M. J. & Gorman, D. J. 1978 Vibration of heat exchanger components in liquid and two-phase cross-flow. In *Proceedings of BNES International Conference on Vibration in Nuclear Plants*, Keswick, England, Paper 2.3.

Pettigrew, M. J. 1981 Flow-induced vibration phenomena in nuclear power station components. *Power Industry Research* **1,** 97–133.

Price, S. J. & Païdoussis, M. P. 1984 A theoretical investigation of the fluidelastic instability of a single flexible cylinder surrounded by rigid cylinders. In *Proceedings of Symposium on Flow-Induced Vibrations*, Vol. 2, (eds M. P. Païdoussis, M. K. Au-yang & S. S. Chen) pp. 117–133. New York: ASME. Also in *ASME Journal of Fluids Engineering* (1986), **108,** 193–199.

Price, S. J. & Païdoussis, M. P. , Mcdonald, R. & Mark, B. 1986 The flow-induced response of the single flexible cylinder in an array of rigid cylinders: A comparison between air- and water-flow results. In *Flow-induced Vibration* 1986, PVP- Vol. 104, Chicago, pp. 107–117. New York: ASME. Also see *Journal of Fluids and Structure* (1987), **1,** 359–378.

Price, S. J. & Païdoussis, M. P. 1987 The flow-induced response of a single flexible cylinder in an in-line array of rigid cylinders. In *Proceedings of a BHRA International Conference on Flow-Induced Vibrations*, Bowness-on-Windermere, England, Paper B1, pp. 51–62.

Rzentkowski, G. 1991 Current-induced vibrations in multi-tube marine riser. Ph. D. Dissertation, Memorial University of Newfoundland, St. John's, Newfoundland, Canada.

Rzentkowski, G. & Lever, J. H. 1992 Modeling of the nonlinear fluidelastic behavior of a tube bundle. In *Proceedings of Symposium on Flow-Induced Vibration & Noise*, Vol. 2 (eds M. P. Païdoussis, S. S. Chen & D. A. Steininger), PVP-Vol. 242, Anaheim, pp. 89–106. New York: ASME.

Singh, K. P. & Soler, A. J. 1984 *Mechanical Design of Heat Exchangers and Pressure Vessels Components.* New Jersey: Arcturus Publishers Inc.

Southworth, P. J. & Zdravkovich, M. M. 1975 Effect of grid turbulence on the fluidelastic vibration of in-line tube banks in cross flow. *Journal of Sounds and Vibration* **39,** 461–469.

Thompson, J. M. T. 1982 *Instabilities and Catastrophies in Science and Engineering.* Chichester, U. K. : John Wiley & Son

Weaver, D. S. & Fitzpatrick, J. A. 1987 A review of flow-induced vibrations in heat exchangers. In *Proceedings of BHRA International Conference on Flow-Induced Vibrations*, Bowness-on-Windermere, England, Paper A1, pp. 1–17.

Zhu, W. Q. & Yu, J. S. 1986 On the response of the Van der Pol oscillator to white noise excitation. *Journal of Sound and Vibration* **117,** 421–431.

APPENDIX: NOMENCLATURE

a	limit-cycle amplitude
c_0	structural damping coefficient
d	tube diameter
f, f_0	frequency of tube oscillation: flow-velocity-dependent and natural, respectively
h	flow resistance coefficient
k_0	structural stiffness coefficients
l_0	tube length
l	relevant fluid inertia length
m, m_0	tube mass: per unit length and effective, respectively
$\bar{m}$	mass parameter, $m/\rho d^2$
$\bar{m}\delta_n, \bar{m}\delta_0$	mass-damping parameter: structural and net, respectively
n	nonlinear solution index
s	position coordinate along streamtube
s_0	distance along streamtube to inlet
t, t_1, t_2	time variable
$y(t), \dot{y}(t), \ddot{y}(t)$	transverse-to-flow tube coordinates: position, velocity and acceleration, respectively
A_0	steady streamtube area at unit-cell inlet
A_{rms}	root-mean-square tube displacement
C_D	drag-dependent force coefficient
C_r, C_r'	random excitation coefficient: dimensional and nondimensional, respectively
D_E	equivalent area of pressure force
F_D	drag-dependent fluid force
F_E	motion-dependent fluidelastic force
F_T	turbulence force
F_{max}	Nyquist frequency
N	nonlinear coefficient
$N_Y(Y)$	average number of cycles required to exceed some value of Y
P	array pitch
T	transverse array pitch
$T(Y)$	tube average return period
T_n	period of tube oscillation
T_{max}	length of turbulence force time series
$S(f)$	power spectral density function
U_0, U_p, U_r, U_u	steady flow velocity: at unit-cell inlet, pitch, reduced and upstream, respectively
Y	tube displacement limit
α	angle defining array pattern
δ	logarithmic decrement of damping
Δf	frequency bandwidth
Δt	time increment
ζ	damping ratio
ρ	fluid density
σ	standard deviation
τ	time lag between tube motion and flow adjustment
ω, ω_0	angular frequency of oscillation: flow-velocity-dependent and natural, respectively